Scientia Africana, Vol. 22 (No. 1), April, 2023. Pp 195-210 https://dx.doi.org/10.4314/sa.v22i1.17

ISSN 1118 – 1931

STATISTICAL MODELLING AND OPTIMIZATION OF FS-WELDED 6061-T651 ALUMINUM ALLOY

Uchegbulam, I.[a*] and Tonye, A. J.[b]
[a]Production Technology, School of Science Laboratory Technology,
University of Port Harcourt, Choba, P.M.B., 5323, Nigeria.
[b]College of Engineering, University of Saskatchewan, Saskatoon, SK S7N 5A9, Canada
*Corresponding author. E-mail address: uche.aberdeen.ac.uk@gmail.com (I. Uchegbulam).

Received: 18-03-2023
Accepted: 06-04-2023

ABSTRACT

An RSM-based experimental design, mathematical modelling and statistical optimization of friction stir welding process parameters was studied. A quadratic fitting model developed from a five-leveled four-factor parametric setting predicted the Ultimate Tensile Strength (UTS) of the welded AA6061-T651 joints. Statistical analysis at 95% Confidence Interval using ANOVA validated the conformity of the developed model with experimental data and also verified the adequacy of the model for UTS prediction and optimization. Results showed that the model was statistically significant ($p<0.0001$) with no notable lack of fit with the four parameters and their squared terms also significant statistically. The numerical optimization resulted to an optimum UTS of 166.32MPa from rotational speed, traversing speed, tool tilt angle and axial load values of 1293.641rpm, 48.467mm/min, 1.888^o and 4.720kN, respectively with a desirability of 0.944. Also, 2D contour and 3D surface plots showed that the four parameters made decreasing effects on the UTS after reaching their optimized UTS. Driving forces for high UTS were: sufficient heat generation for plastic deformation, effective material coalescence, appropriate extrusion of molten material towards the trailing edge, adequate heat and mass transfer to control grain coarsening, void and flash formations. With an SN-ratio of 45.963 and low coefficient-of-variation of 1.11%, the conformity of the predicted and adjusted regression coefficients (R^2) of 0.9619 and 0.9868 respectively supported by the confirmatory test and diagnostic plots showed a strong correlation between the experimental and predicted results. These demonstrated that the developed model was sufficient for predicting and optimizing the UTS of Friction Stir Weld (FSW) AA6061T651 plates.

Keywords: friction stir welding, Response surface methodology (RSM), modelling, optimization

INTRODUCTION

The necessity to maximize cargo at minimal fuel consumption has been an issue that has recently caught the attention of both the industrial and academic communities. Engineering materials with a high specific strength due to a good blend of their light weight and structural strengths are strong contenders of this application. Top ranking alloys on the specific strength table are Titanium, Aluminum and Magnesium alloys with the universal Aluminum grades: AA5052, AA6061, AA7075 being the most popular. This made them to be widely used in the automobile, aerospace, marine, construction, railway, nuclear, electronic, defense, offshore oil and gas industries due to their excellent properties compared to other competing materials, (Karimi-Dermani, et al., 2021; Roeen, et al., 2021; Sezhian, et al., 2021). In assembling these structural components, welding has become an indispensable industrial joining process especially when size and complexity matters.

However, fusion welding of Aluminum alloys has met several challenges due to the toughness of its tenacious oxide layer, high degrees in thermal conductivity and linear expansivity as well as rapid rates of solidification and dissolved Hydrogen solubility, [Roeen, et al., 2021; Sezhian, et al., 2021]. Common defects arising from fusion welding of Aluminum alloys includes: development of residual stresses, high porosity, oxide inclusion, distortion, coarse and brittle dendritic grain structures. Also, hot cracking and softening of both the FZ (fusion zone) and the Heat Affected Zone (HAZ) are common in fusion weld Aluminum alloys. Friction Stir Welding (FSW) as a solid-state welding technology was developed at The Welding Institute (TWI), Cambridge, UK, [Kumar, et al., 2022], to overcome these welding challenges. As an environmentally-friendly and energy saving welding technology, [Salah, et al., 2022], FSW has been attracting much interest in both the research and industrial communities in the welding of materials with unrelated physical, metallurgical and mechanical properties. Meanwhile, the FSW joint integrity principally depends on the process parameters. These parameters depend on the nature and conditions of the non-consumable welding tool such as the tool's angle of tilt, diameter, configurations, axial force, Plunge depth, rotational speed and welding speed. Recently, the combination of mathematical and statistical tools in FSW process modelling and optimization is recently gaining wider recognition in the academia and manufacturing industries. This can be linked to the reduced experimental runs for multi-parameter investigations leading to simplicity, time savings with higher reliability and of course, makes economic sense. The present study focused on AA6061-T651 as a variant of the popular AA6061-T6 universal Aluminum alloy. Many researchers have studied the FSW of AA6061 alloys especially as dissimilar joints. For instance, at 95% statistical confidence interval (CI) with AA6082 in a dissimilar joint with the AA6061, [Kumar, et al., 2021], FSW parameters were optimized at 1.89^{o}, 45.92 mm/min and 1178.2 rpm for tilt angle, welding and rotational speeds respectively leading to UTS, hardness and strain of 205.64 MPa, 105.35 HV and 18.97% accordingly. At same 95% CI, [Salah, et al., 2022], optimized FSW parameters at 1.252o tilt angle, 1172 rpm and 57.44 mm/min rotational and welding speeds led to 74.47 hardness, 12.18% ductility and 95.8 MPa UTS. Also, by welding AA5082 and AA6061 together, [Ramana, et al., 2021], used a taper trapezoidal pin to optimize a 3.38% ductility, UTS of 157.33 MPa, 78.5 RHC and yield strength of 123.36 MPa from rotational speed of 1600 rpm and welding speed of 20 mm/min. Furthermore, UTS of AA6061 joined with Titanium alloy was predicted in [Rahiman, et al., 2022] by combining RSM and Artificial Neural Network (ANN). A maximum error between the actual and predicted results at 1.01%. showed the reliability of the developed model. Likewise, [Rathinasuriyan, and Kumar, 2021] used the combination of RSM with Grey Relation Analysis (GRA) to optimize 88.42 Hardness and 28.18 % ductility from a water head of 10 mm, rotational and welding speeds of 1200 rpm and 30 mm/min respectively. These studies used mathematical models to predict the multi-factorial effects on a targeted result or response. Many studies have investigated the effects and interactions of tool's rotational and welding speeds in addition to one extra parameter while investigating up to four parameters is hereby studied for the first time. Hence, this RSM-based modelling and optimization of FS-

Scientia Africana, Vol. 22 (No. 1), April, 2023. Pp 195-210 https://dx.doi.org/10.4314/sa.v22i1.17
© Faculty of Science, University of Port Harcourt, Printed in Nigeria ISSN 1118 – 1931

Welded AA6061-T651 aimed at predicting the UTS by formulating the ideal FSW set of four parameters, establishing their effects on the dependent variable as well as interactions with one another.

EXPERIMENTAL PROCEDURE

Materials

Pre-tempered grade AA6061 plates of $120x120x5mm^3$ were obtained from an Aluminum extrusion company at Port Harcourt, Nigeria. These T651 tempered plates were used in the As-received condition of solution heat-treated, stress relieved and artificially aged without further modification. This general-purpose Aluminum Alloy (AA) grade was preferred for its high weldability, good mechanical properties with excellent acceptance of applied coatings.

Methods

The AA6061-T651 characterization was carried out by energy dispersive X-Ray Fluorescence analysis using Oxford Instrument X-Met 7000 XRF Spectrometer (Oxford Instruments plc, England, UK) according to our previous study (Uchegbulam, et al., 2019) at different positions on the plate and was observed to be precise. The XRF results are shown in table 1:

Table 1: The elemental composition of the Aluminum alloy used:

Mg	Si	Cu	Cr	Fe	Zn	Ti	Mn	Al
0.91	0.62	0.32	0.27	0.26	0.23	0.17	0.14	Balance

Single pass FSW runs were carried out on a modified vertical milling machine after adequate clamping was done to arrest all degrees of freedom. The rotating non-consumable High-speed-steel tool with a square pin on a cylindrical shank profile was driven into the butt joint until the plate surface makes contact with the tool's shoulder. After a dwell time for plastic flow, the tool was made to travel along the joint perpendicular to the extrusion direction of the plates. Dog-bone shaped samples of $100 \times 10 \times 2$mm in length, width and thickness respectively were cut from the in a way that the gauge length was within the weld nugget. Using EZ 250 AMETEK Twin column Bench mounted Tensile testing machine, (Lloyd Instruments, USA), shown in figure 1. Tensile test was conducted according to ASTM E8 standard. Uniaxial loads were carried out at ambient conditions to obtain the Ultimate tensile strength (UTS) of the samples and results recorded accordingly.

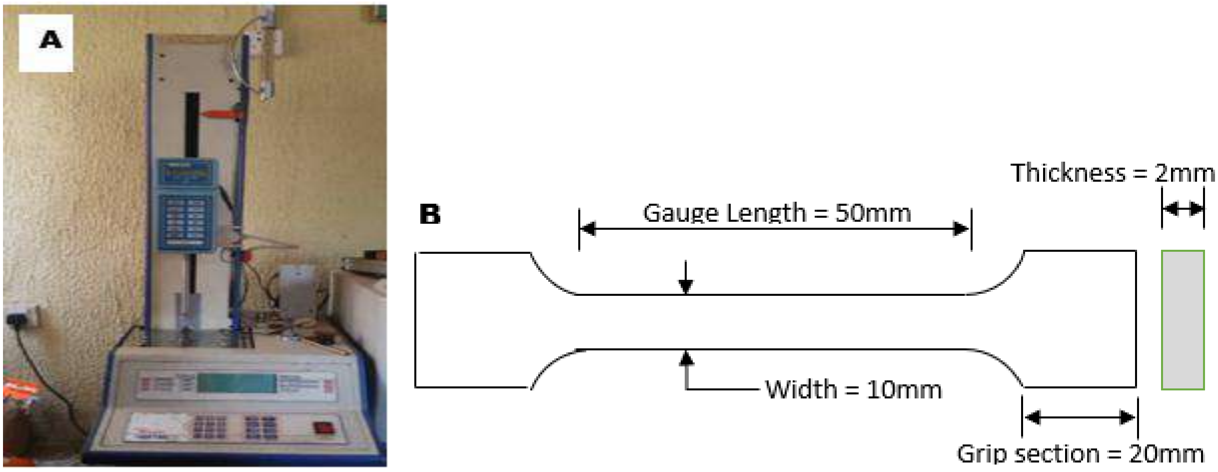

Figure 1: (A) Tensile testing machine used (B) Schematic diagram of tensile test samples

Design of experiment

To model and optimize the Ultimate Tensile Strength (UTS) of the FSWed joints, four major FSW parameters were studied: Welding tool's rotational speed (R_S in rpm), transversing or welding speed (W_S in mm/min), Axial load (A_L in kN) and tool's angle of tilt (T_A in ^{o}). A second order (quadratic) mathematical regression model predicting the individual and interactive effects of these four independent variables was established as they relate to the UTS as the response variable. To minimize empirical runs, the experiment was arranged using Design of Experiment (DOE) in DesignExpert Version 13 using the Central Composite Design (CCD) method of Response surface methodology (RSM). With each of the four numeric factors set to 5 levels: ± α (axial points), ± 1 (factorial points) and the center point led to 30 runs consisting 6 and 24 center points and non-center points respectively. The design window was built in two blocks and replicates of the two blocks. It was also set at upper and lower limits using α = ± 2 in line with [Rahiman, et al., 2022], while the intermediaries were obtained using:

$$X_i = 2\,[2X - (X_{max} + X_{min})] / (X_{max} + X_{min}) \quad \ldots\ldots\ldots\ldots\ldots\ldots\ldots\ldots\ldots\ldots[1]$$

Where X_i is the particular coded value needed for variable X while X is a variable between X_{max} and X_{min}. This was used to establish the design space shown in tables 2 for the experiment.

Table 2: Parametric Design Window

Process Parameters	Unit	Symbol	Levels (α = 2)				
			-α	-1	0	1	A
Tool rotational speed	(rpm)	R_s	1350	1500	1650	1800	1950
Welding Speed	(mm/min)	W_s	15	40	65	90	115
Axial Load	(kN)	A_L	3	5	7	9	11
Tilt Angle	(^{o})	T_A	0	1	2	3	4

Development of mathematical model

The response variable is related to the independent variables following the equation:

$$Y = f\,(X_1, X_2, \ldots\ldots\ldots, X_n) \pm \varepsilon \quad \ldots\ldots\ldots\ldots\ldots\ldots\ldots\ldots\ldots\ldots[2]$$

Scientia Africana, Vol. 22 (No. 1), April, 2023. Pp 195-210 https://dx.doi.org/10.4314/sa.v22i1.17
© Faculty of Science, University of Port Harcourt, Printed in Nigeria ISSN 1118 – 1931

where Y is the response variable (UTS) as a function (f) of the independent variables: x_1, x_2 up to X_n while n is the number of the independent variables. In this study, n=4 and x_1, x_2, x_3 and x_4 are the tool's rotational speed (R_S), welding speed (W_S), Axial load (A_L) and tool's angle of tilt (T_A) respectively. The function (f) is equivalent to the response surface because it proportionately relates to the set of independent variables. In this study, the RSM treats the independent variables as surfaces on which a mathematical regression model can be fitted to predict the response variable within the experimental design space. These are within the limits of experimental errors denoted by the residual error (ε) estimated by the sum of squared deviations of the experimental from the predicted responses:

$$Y = \beta_0 + \sum_{i=1}^{k} \beta_i x_i + \sum_{i=1}^{k} \beta_{ii}^2 x_{ii}^2 + \sum_{i<j}^{k} \beta_{ij} x_i x_{ij} + \varepsilon \quad \ldots\ldots\ldots\ldots\ldots\ldots\ldots\ldots [3]$$

Where Y is the response variable, x is n^{th} independent variable for k number of variables, $\boldsymbol{\beta}_0$ is the intercept which is equivalent to the mean value of the response, ε is the residual error while $\boldsymbol{\beta}_i$, $\boldsymbol{\beta}_{ii}$ and $\boldsymbol{\beta}_{ij}$ are respectively the linear, quadratic and interaction coefficients.

This will offer a designed quadratic regression model of the form:

$$Y = a_0 + b_1R_S + b_2W_S + b_3A_L + b_4T_A + b_{11}R_{S2} + b_{22}W_{S2} + b_{33}A_{L2} + b_{44}T_{A2} + b_1b_2R_SW_S + b_1b_3R_SA_L$$
$$+ b_1b_4R_ST_A + b_{23}W_SA_L + b_2b_4W_ST_A + b_3b_4A_LT_A \ldots\ldots\ldots [4]$$

where Y is the UTS (MPa), R_S is the tool's rotational speed (rpm), W_S is the welding speed (mm/min), A_L is the Axial load (kN), T_A is the tool's angle of tilt (^{o}) while the value of the coefficients is estimated from analytical methods.

Response optimization and confirmation

Optimization was ramped for a maximum UTS at the experimental lower limit of 116.98MPa and stretched to the upper limit of 166.03MPa. The numerical optimization was run at the default settings of 100 number of solutions with 50 design points at 0.1 simplex fraction and to obtain the desirability objective function, the optimization was linearly weighted (weights of 1) and maintained the default of 3 degrees of importance assigned to the goal as shown in table 3.

Table 3: Constraints for numerical optimizations criteria

Variable	**Units**	Goal	Lower Limit	Upper Limit	Lower Weight	Upper Weight	Importance
A:Rs	Rpm	is in range	1200	1500	1	1	3
B:Ws	mm/min	is in range	40	60	1	1	3
C:Ta	Degree	is in range	1	3	1	1	3
D:Al	kN	is in range	3	7	1	1	3
UTS	MPa	maximize	116.98	166.03	1	1	3

In addition, a two-sided confirmatory run at 95% CI. was conducted with the confirmatory test result to investigate the variability of the predicted and actual confirmatory results.

RESULTS

Model formulation

Using the established design, the experiment was carried out in the run order of the design matrix in uncoded independent variables (Table 4) showing the experimental and predicted UTS from the 30 runs. This was used to develop the second-order polynomial (quadratic) model of the UTS (equation 5).

$$\mathbf{UTS} = -731.91299 + 1.07905\,\mathbf{R_S} + 6.24737\,\mathbf{W_S} + 30.32271\,\mathbf{T_A} + 7.29865\,\mathbf{A_L} + 0.000036\,\mathbf{R_S} * \mathbf{W_S} - 0.005467\,\mathbf{R_S} * \mathbf{T_A} + 0.004\,\mathbf{R_S} * \mathbf{A_L} - 0.056\,\mathbf{W_S} * \mathbf{T_A} - 0.028625\,\mathbf{W_S} * \mathbf{A_L} + 0.040625\,\mathbf{T_A} * \mathbf{A_L} - 0.000421\,\mathbf{R_S}^2 - 0.062444\,\mathbf{W_S}^2 - 5.49187\,\mathbf{T_A}^2 - 1.18266\,\mathbf{A_L}^2 \qquad [5]$$

Table 4: Experimental design matrix and the response variable

Run No.	Independent Variables				Experimental Result	Predicted Result	Error
	R_S (rpm)	**W_S (mm/min)**	**T_A (°)**	**A_L (kN)**	**UTS (MPa)**	**UTS (MPa)**	**%**
1	1200	40	3	3	141.87	147.58	4.02
2	1350	50	2	5	156.02	163.54	4.82
3	1500	40	1	7	127.03	135.61	6.75
4	1500	60	3	7	118.01	125.78	6.58
5	1500	60	3	3	118.03	126.27	6.98
6	1200	40	3	7	138.98	144.57	4.02
7	1500	60	1	7	123.11	131.63	6.92
8	1200	40	1	7	138.92	144.9	4.30
9	1500	40	3	3	122	130.2	6.72
10	1200	60	1	3	139.98	146.32	4.53
11	1500	40	3	7	124.12	131.99	6.34
12	1200	40	1	3	141.97	148.23	4.41
13	1350	50	2	5	158.83	163.54	2.97
14	1200	60	3	3	137.98	143.43	3.95
15	1200	60	3	7	130.1	138.14	6.18
16	1500	40	1	3	127.95	134.14	4.84
17	1350	50	2	5	156.92	163.54	4.22
18	1500	60	1	3	124.01	132.45	6.81
19	1200	60	1	7	134.88	140.7	4.31
20	1350	50	2	5	156.98	163.54	4.18
21	1350	50	2	1	149.1	146.53	-1.72
22	1350	70	2	5	138.93	134.5	-3.19
23	1650	50	2	5	116.98	112.51	-3.82
24	1350	50	2	5	166.03	163.54	-1.50
25	1350	30	2	5	145.01	142.63	-1.64
26	1350	50	0	5	148.02	144.82	-2.16
27	1350	50	2	5	165.11	163.54	-0.95
28	1350	50	2	9	146.95	142.7	-2.89
29	1050	50	2	5	141.13	138.96	-1.54
30	1350	50	4	5	141.94	138.32	-2.55

Scientia Africana, Vol. 22 (No. 1), April, 2023. Pp 195-210 https://dx.doi.org/10.4314/sa.v22i1.17
© Faculty of Science, University of Port Harcourt, Printed in Nigeria ISSN 1118 – 1931

Verification of developed model adequacy

At a confidence interval of 95%, the statistical significance of the goodness of fit of the prediction model (equation 5) was tested using ANOVA.

Table 5: ANOVA for Quadratic model

Source	Sum of Squares	df	Mean Square	F-value	p-value
Block	671.41	1	671.41		
Model	5062.46	14	361.60	150.95	< 0.0001*
A-Rs	1186.10	1	1186.10	495.13	< 0.0001*
B-Ws	99.63	1	99.63	41.59	< 0.0001*
C-Ta	63.12	1	63.12	26.35	0.0002*
D-Al	21.93	1	21.93	9.15	0.0091*
AB	0.0462	1	0.0462	0.0193	0.8915**
AC	10.76	1	10.76	4.49	0.0524**
AD	23.04	1	23.04	9.62	0.0078*
BC	5.02	1	5.02	2.09	0.1698**
BD	5.24	1	5.24	2.19	0.1611**
CD	0.1056	1	0.1056	0.0441	0.8367**
A^2	2461.44	1	2461.44	1027.50	< 0.0001*
B^2	1069.50	1	1069.50	446.45	< 0.0001*
C^2	827.26	1	827.26	345.33	< 0.0001*
D^2	613.82	1	613.82	256.23	< 0.0001*
Residual	33.54	14	2.40		
Lack of Fit	28.94	10	2.89	2.52	0.1937**
Pure Error	4.60	4	1.15		
Cor Total	5767.41	29			

*Significant **Not Significant at 95% Confidence limit

From table 5, the quadratic model's F-value of 150.95 and p-value less than 0.0001 demonstrates that the model is significant. Statistically, there is only a 0.01% chance that an F-value this large could occur due to noise. Interestingly, table 5 shows an F-value of 2.52 and p-value of 0.1937 for the model's Lack of Fit. This 19.37% which is greater than the standard 10% indicates that the Lack of Fit is not significant (this means that the model's fit for prediction is significant) relative to the pure error.

Furthermore, other significant model terms with p-values lower than 0.05 were A, B, C, D, AD, A^2, B^2, C^2, D^2 representing the rotational speed, welding speed, angle of tilt, axial force, and interaction between the rotational speed and axial force as well as their squared values respectively. This demonstrated that all the selected FSW parameters play significant roles In optimizing the UTS of the weld integrity. Remarkably, this result indicates a strong interaction between the axial load on the tool and the tools rotational speed and this interaction has a significant impact on the UTS of FSW of AA6061-T651 joints.

Furthermore, table 6 shows the fit statistics of the experiment.

Table 6: Experimental Fit statistics

Std. Dev.	1.55		R^2	0.9934
Mean	139.23		**Adjusted R^2**	0.9868
C.V. %	1.11		**Predicted R^2**	0.9619
			Adeq Precision	45.9625

From table 6, the Predicted regression coefficient (R^2) of 0.9619 is in practical conformity with the Adjusted R^2 of 0.9868 since their difference is below the statistical limit of 0.2. These results show a strong correlation between the experimental data and predicted values. Also, a low coefficient-of-variation (CV) value of 1.11% was recorded indicating a very high degree of accuracy for determining the UTS of FSWed joints using a combination of these parameters. In addition, as the Adequate (Adeq) Precision calculates the S-N ratio (signal to noise ratio), the model's S-N ratio of 45.963 is a satisfactory signal far greater than the standard threshold of 4.00. These results are strong indications that the developed quadratic model is adequate to navigate the experimental design space for estimating the UTS of the FSWed joints.

Residual analysis

Diagnostic analysis of the designed model's properties is another measure for verifying the RSM model's fitness for predicting the UTS of FSWed AA6061-T651 joints. These were done by characterizing the model's residuals by plotting the externally studentized residuals as shown in figure 4. Figure 2a shows the residuals and the distribution of their fitted values. It can be noticed that the points are closely fitted around the regression line with a normal distribution similar to the results in [Rahiman, et al., 2022]. Figure 2b shows that the positive and negative residuals were spread around the zero line in an indistinguishable pattern apart from two noticeable outliers at runs 23 and 29 corresponding to the extreme (lower and upper) limits of the axial ($\pm \alpha$) points. Figure 2c shows a linear correlation between the predicted and experimental data with minimal variation. The Box-Cox plot was used as a diagnostic tool that recommended the appropriate power law transformation. The Box-Cox plots (Figure 2d) at the default range of $\pm 3\lambda$ indicates a low confidence interval of 0.71 (red line) with the green line signifying the best or optimum lambda value of 2.35 and blue line representing the current Lambda value of 1. Since the optimum lambda line (blue) lies between the lower and upper C.I. lines (red), this means that the model is properly fitted to the experimental data presented as obtained in [Tong, et al., 2022; El-Naggar and El-Shweihy, 2020]. More importantly, since the lower and upper C.I. limits accommodates the optimum lambda value of 1, this demonstrates a distribution normality hence no need for power transformation of the obtained data to obtain variance stability.

Scientia Africana, Vol. 22 (No. 1), April, 2023. Pp 195-210 *https://dx.doi.org/10.4314/sa.v22i1.17*
© Faculty of Science, University of Port Harcourt, Printed in Nigeria *ISSN 1118 – 1931*

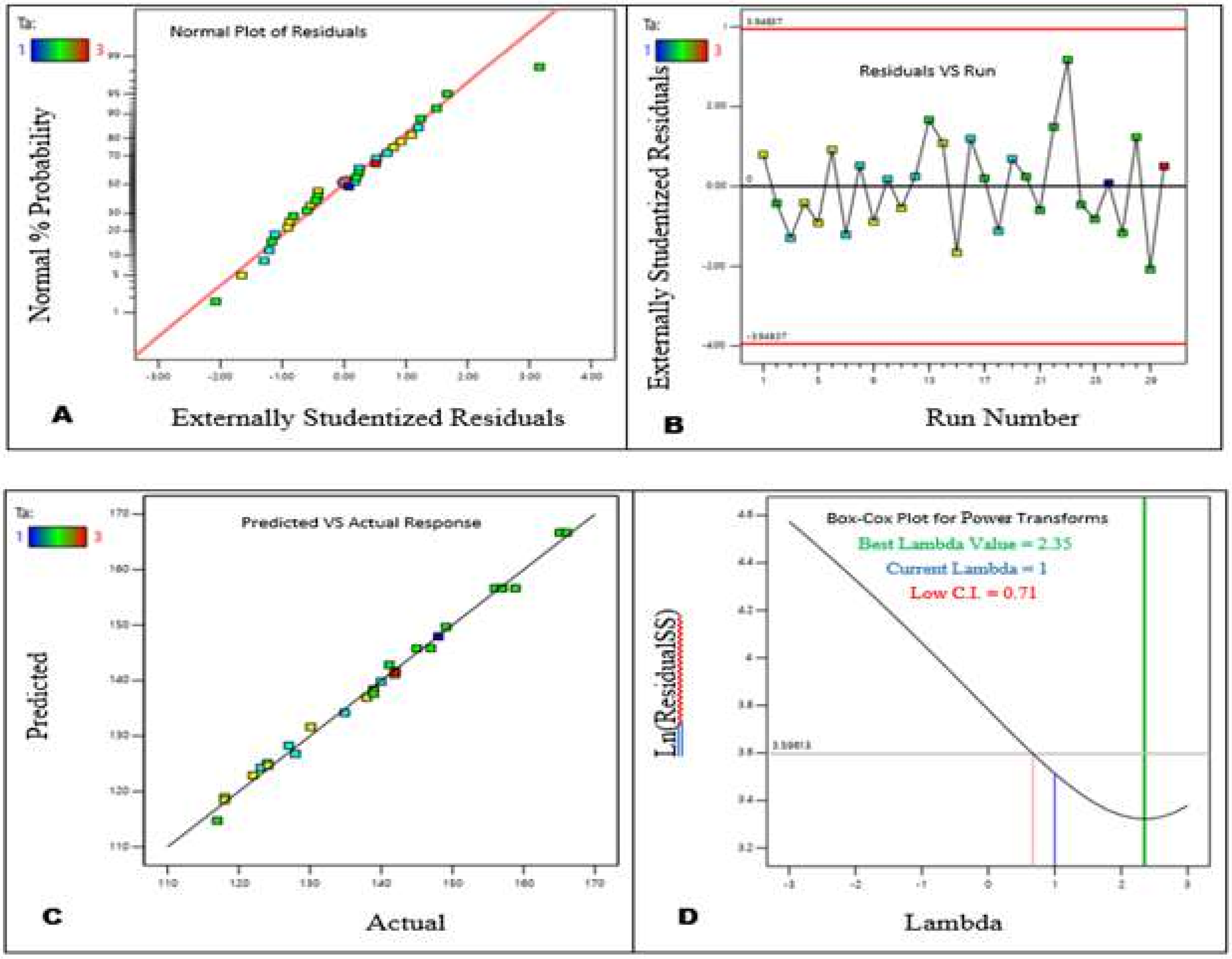

Figure 2: Residual plots: (A) Normal probability plot of residuals (B) Plot of residuals versus experimental run (C) Plot of predicted versus actual data (D) Box-cox Plot for power transforms.

Hence, these diagnostic plot conditions and their homoscedasticity in agreement with the R^2 values demonstrate the RSM model's adequacy in predicting the UTS of the FSWed joint.

Influence of parameters

To study the parametric influence of Ta, Rs, Ws and Al on the response variable (UTS), two of the four factors were fixed at their central points, the other two were drawn on the x and z-axis while the response variable was plotted on the y-axis.

Based on this, as both the TA and AL were set at 2^o and 5kN respectively, a combination of Rs and WS were presented in the Contour and 3D surface plots in figure 3a and 3b respectively. Optimal UTS values were available as Rs was between 1207.69 to 1379.93rpm for heat generation when combined with Ws from 41.24 to 55.48mm/min as the ideal material flow speed. This result is in line with [Salah, et al., 2022]. The result also shows that heat generated below 1207.69rpm will not be enough for FSW while excessive plastic deformation that lowers UTS will occur at TS above 1379.93rpm. In addition, the result also demonstrates that Ws below 41.24mm/min will be too slow for material mixing leading to excessive dwell time that cause undesirable heat treatments like grain coarsening which consequently reduces the UTS. Also, Ws above 55.48mm/min will be an excessive material mixing which can generate microvoids [Mohan, et al., 2021] and flashes responsible for lower UTS.

As more particles interact under larger surface area, more frictional heat can be generated. This can be linked to the case of higher plastic deformation under the tool shoulder than around the tool pin showing that tilt angle effect on heat generation and material flow are prominent at the shoulder than at the pin as supported by [Omar, et al., 2023]. In addition, the collective impacts of the axial force, rotational speed and welding speed and their directions give rise to a localized downward forging force on the molten material towards the trailing edge. At zero tilt angle, the material flow and temperature distribution may be symmetric around the welding tool and sufficient to plastically deform the materials for FSW. However, there will be a temperature gradient between the Advancing side (AS) and the retreating side (RS) leading to differential heat and mass transfer that causes void formation towards the RS.

By tilting the tool (increasing Ta) as shown in the Contour and 3D surface plots in figure 3c and 3d, less materials are transported and heat flux increases thereby reducing viscosity and allowing the plastic material to flow and fill potential voids. In those figures (3c and 3d), appropriate tilt angles between 1.29 to 2.42^{o} at Axial loads from 3.56 to 6.05kN are required for optimal UTS of 165.11MPa. Within these parameters, suitable heat flux and material flow extrude plasticized materials into weld defects and the nugget is consolidated by the axial force to form high UTS joints. However, at excessive tilt angles, the axial force concentrates on a less area thereby increasing the frictional force, hence, heat for FSW. However, at high Ta, the nose of the tool shoulder is raised at the leading edge, deeply submerged at the trailing edge and this reduces the tool-material contact area. As the axial force concentrates on a less area, both the forging pressure and heat flux increases leading to a turbulent flow field emerging as weld flash which are extruded in the Rs direction. This is why the generated flashes emerge from the Rs with an asymmetric heat flux between the leading and retreating sides of the weld seam. The flash sputtering causes material deficiency as required for filling the weld nugget. This material deficit causes reductions in UTS, weld thickness and surface finish. This trend agrees with results in [Acharya, et al., 2021].

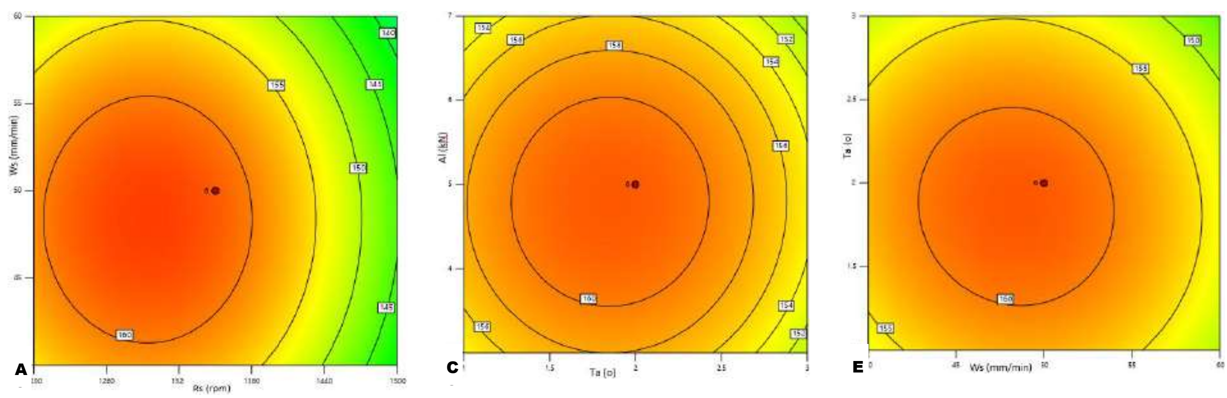

Scientia Africana, Vol. 22 (No. 1), April, 2023. Pp 195-210 https://dx.doi.org/10.4314/sa.v22i1.17
© Faculty of Science, University of Port Harcourt, Printed in Nigeria ISSN 1118 – 1931

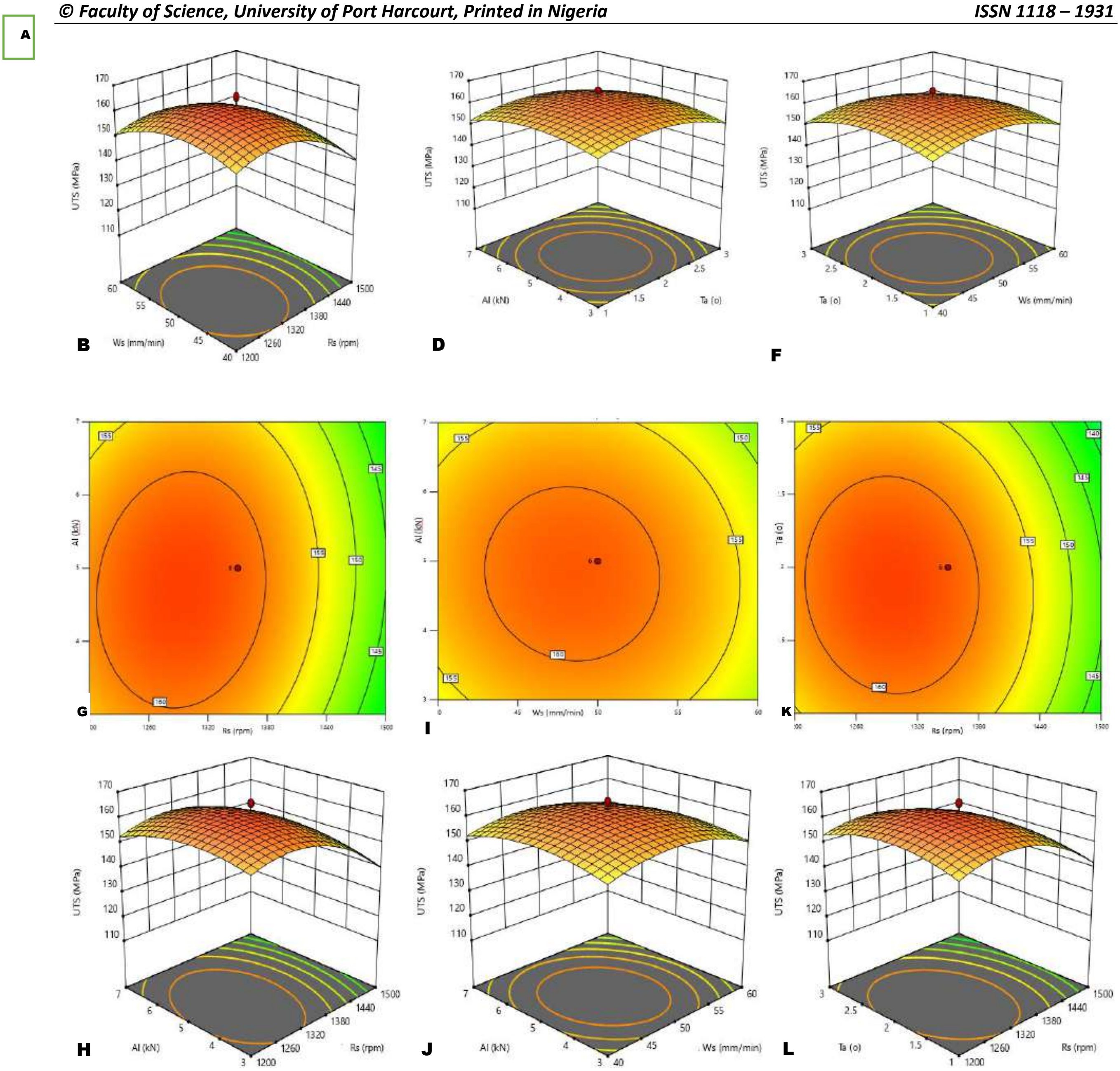

Figure 3: Contour and surface plots of FSW process parameters effects on UTS

A similar trend as reported in [Kumar, et al., 2021;], can be noticed in figure 3e and 3f where the UTS of the weld nugget increased as the combination of Ta and Ws increases to optimal settings of 1.27 to 2.45^{o} and 42.86 to 54.01mm/min for Ta and Ws respectively. Outside theses ranges, the UTS was lowered due to weld defects and flashes. Similarly, the combinations of axial load and rotational speed at optimal settings between 3.08 to 6.32kN and 1206.83 to 1379.07rpm for Al and Rs respectively in figure 3g and 3h at fixed settings of both the traversing speed and tilt angle positively improved UTS of the joint. This can be linked to sufficient heat generation necessary for plastic deformation which in excess negatively affects the UTS as recorded in [Salah, et al., 2022].

In addition, figure 3i and 3j showed that axial loads between 3.55 to 6.97kN and transverse speeds from 42.93 to 53.88mm/min can achieve high UTS weld joints when the tilt angle and rotational speed are fixed at their central points of 2^{o} and 1350rpm respectively.

Likewise, figure 3k and 3l showed the blend of tilt angle and rotational speed between 1.13 to 2.62^{o} to 1210.30 to 1381.64rpm at fixed values of welding speed and axial load. This show that outside these parametric ranges, the UTS reduces due to insufficient heat generation, void and flash formations.

In addition, the contour plots demonstrated two types of shapes: concentric (Figure 3a,c,e and i) and elliptical (Figure 3g and 3j) contour lines. It is known that concentric contour plots demonstrate that the parameters affect the response independently while the elliptical contour plots reveal that the parameters affect the response variable simultaneously which is also a measure of interaction between the factors. This is also supported by the p-values of the factors in figure 3g and 3j for interactions: Al-Rs (p=0.0078) and Ta-Rs (p=0.0524) respectively. Furthermore, the ellipticity of Al-Rs lines are more than those of Ta-Rs showing that their interaction was stronger as supported by their statistical significance of these p-values validated in table 5.

Optimization and confirmation

The numerical optimization result of the RSM model yielded a one-optimized-solution showing how well the optimization goal was met. Figure 4 showed that the UTS was maximized to 163.289MPa with corresponding values of Rs, Ws, Ta and Al at 1293.641rpm, 48.467mm/min, 1.888o and 4.720kN respectively. Also, a desirability of 0.944 shown in figure 4 was obtained showing that the response was within acceptable limits as a majority of the design space matched the criteria selected.

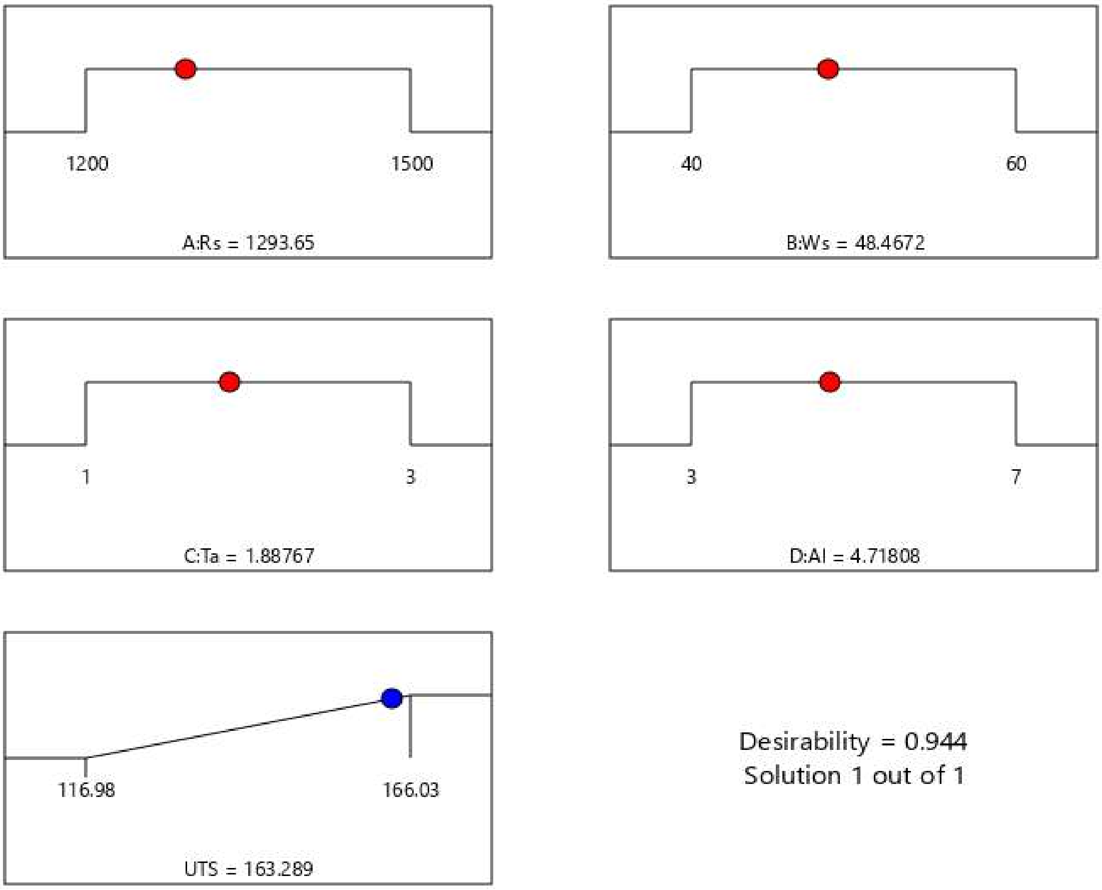

Figure 4: Numerical optimization solution ramps of the parameters and UTS response

Scientia Africana, Vol. 22 (No. 1), April, 2023. Pp 195-210 *https://dx.doi.org/10.4314/sa.v22i1.17*
© Faculty of Science, University of Port Harcourt, Printed in Nigeria *ISSN 1118 – 1931*

A confirmatory test was run using the optimized results, as shown in table 7. The results show a 2.16% deviation between the predicted and confirmed runs. The degree of agreement is a validation of the optimized results by the confirmatory runs which is highly acceptable for practical operation of AA6061 joints FSW.

Table 7: confirmatory test results

Variable	Rs (rpm)	Ws (mm/min)	Ta (^{o})	Al (kN)	UTS (MPa)
Optimized	1293.641	48.467	1.888	4.720	163.289
Confirmation	1293.641	48.467	1.888	4.720	159.831
Error	-	-	-	-	2.16 %

This was also used to run a two-sided numerical confirmatory test at 95% CI., the result was satisfactory with no variability as there the experimental result was within the numerical lower and upper CI limits of 159.707 and 166.87MPa respectively.

CONCLUSION

In this study, a four-factor with five-leveled Central Composite Design based Response Surface Methodology was used to draw a 30-run experimental design space from which data for a quadratic model was developed using Design-Expert 13 statistical software. Statistical analysis using ANOVA validated the conformity of the developed quadratic model with experimental data and also verified the adequacy of the model in predicting and optimizing the UTS of FSWed AA6061T651 plates at 95% Confidence Interval within the experimental design space. It was noticed that the driving forces for weld integrity includes sufficient heat generation for plastic deformation, effective material coalescence, appropriate extrusion of molten material towards the trailing edge, adequate heat and mass transfer to control grain coarsening, void and flash formations.

With no data transformation carried out based on Box-Cox plots recommendations, diagnostic analysis of the designed model plotted its externally studentized residuals and revealed a normal distribution with the points closely fitted around the regression line.

Also, the goodness of fit of the prediction model showed that the model was statistically significant ($p<0.0001$). This analysis also indicated that all of the four parameters (rotational speed, traversing speed, tool tilt angle and axial load) and their squared terms were also significant statistically. Remarkably, the combination of Rs and Al were statistically significant with p-value of 0.0078 showing the strong interactive effect the factors made on the UTS as supported by their very elliptical contour lines. 2D contour and 3D surface plots showed that the four parameters made decreasing effects on the UTS after reaching their optimized UTS.

Using the desirability approach, a numerical optimization ramped for a maximum UTS resulted to optimum UTS of 166.32MPa from rotational speed, traversing speed, tool tilt angle and axial load values of 1293.641rpm, 48.467mm/min, 1.888^o and 4.720kN respectively. In addition, a desirability of 0.944 was obtained showing that the optimized UTS was within acceptable limits of the C.I. as majority of the design space matched the goal criteria selected.

In addition, with no notable lack of fit, a strong correlation between the experimental and predicted results was also demonstrated through the conformity between the predicted and adjusted regression coefficient (R^2) of 0.9619 and 0.9868 respectively. Also, the model's S-N ratio of 45.963 and low coefficient-of-variation of 1.11% are indicators of high degree of modelling accuracy. Furthermore, the conformity of this validated model with experimental data supported by the confirmatory test and diagnostic plots show that the developed RSM-based model was sufficient for predicting and optimizing the UTS of FSWed AA6061T651 plates.

REFERENCES

Acharya, U., Roy, B.S. and Saha, S.C., 2021. *On the Role of Tool Tilt Angle on Friction Stir Welding of Aluminum Matrix Composites," Silicon, Vol. 13, pp. 79–89,* view online.

El-Naggar, N.E. and El-Shweihy, N.M., 2020. *"Bioprocess Development For L-Asparaginase Production by Streptomyces Rochei, Purification and In-Vitro Efficacy Against Various Human Carcinoma Cell Lines," Scientific Reports, Vol. 10, No. 7942,* view article online.

Karimi-Dermani, O., Abbasi, A., Roeen, G.A. and Nayyeri, M.J., 2021. *"Dissimilar Friction Stir Lap Welding of AA7075 To AZ31B in the Presence of Sn Interlayer," Journal of Manufacturing Processes, Vol. 68, p. 616–631,* view article online

Kumar, J., Majumder, S., Mondal, A.K. and Verma, R.K., 2022. *"Influence of Rotation Speed, Transverse Speed, And Pin Length During Underwater Friction Stir Welding (UW-FSW) on Aluminum AA6063: A Novel Criterion for Parametric Control," International Journal of Lightweight Materials and Manufacture, Vol. 5, pp. 295-305,* view article online.

Kumar, R., Dhami, S.S. and Mishra, R.S., 2021. *"Optimization of Friction Stir Welding Process Parameters During Joining of Aluminum Alloys of AA6061 and AA6082," Materials Today: Proceedings, Vol. 45, p. 5368–5376,* view article online.

Mohan, D.G., Tomków, J. and Gopi, S., 2021. *"Induction Assisted Hybrid Friction Stir Welding of Dissimilar Materials AA5052 Aluminium Alloy and X12CR13 Stainless Steel," Advances in Materials Science, Vol. 21, No. 3, pp. 17-30,* view article online.

Omar S. S., Ou, H. and Sun, W., 2023. *"Heat Generation, Plastic Deformation and Residual Stresses in Friction Stir Welding of Aluminium Alloy," International Journal of Mechanical Sciences, Vol. 238, pp. 1-16,* view article online.

Rahiman, M.K., Santhoshkumar, S., Mythili, S., Barkavi, G.E., Velmurugan, G. and Sundarakannan, R., 2022. *"Experimental Analysis of Friction Stir Welded of Dissimilar Aluminium 6061 and Titanium TC4 Alloys Using Response Surface Methodology (RSM)," Materials Today: Proceedings, Vol. 66, p. 1016–1022,* view article online.

Ramana, G.V., Yelamasetti, B. and Vardhan, T. V., 2021. *"Effect of FSW Process Parameters and Tool Profile on Mechanical Properties of AA 5082 and AA 6061 Welds," Materials Today: Proceedings , Vol. 46, p. 826–830,* view article online.

Rathinasuriyan, C. and Kumar, V.S.S. 2021. *"Optimisation of Submerged Friction Stir Welding Parameters of Aluminium Alloy*

Scientia Africana, Vol. 22 (No. 1), April, 2023. Pp 195-210 https://dx.doi.org/10.4314/sa.v22i1.17
© Faculty of Science, University of Port Harcourt, Printed in Nigeria ISSN 1118 – 1931

Using RSM and GRA," Advances in Materials and Processing Technologies, Vol. 7, No. 4, pp. 696-709, view article online.

Roeen, G.A., Yousefi, S.G., Emadi, R., Shooshtari, M. and Lotfian, S., 2021. *"Remanufacturing the AA5052 GTAW Welds Using Friction Stir Processing," Metals, Vol. 11, No. 749, pp. 1-13,* view article online.

Salah, A.N., Mehdi, H., Mehmood, A., Hashmi, A.W., Malla, C. and Kumar, R., 2022. *"Optimization of Process Parameters of Friction Stir Welded Joints of Dissimilar Aluminum Alloys AA3003 and AA6061 by RSM," Materials Today: Proceeding, Vol. 56, p. 1675–1683,* view article online.

Sezhian, M.V., Giridharan, K., Pushpanathan, D.P., Chakravarthi, G., Stalin , B., Karthick , A., Kumar, P.M. and Bharani, M., 2021. *"Microstructural and Mechanical Behaviors of Friction Stir Welded Dissimilar AA6082-AA7075 Joints," Advances in Materials Science and Engineering, Vol. 2021, No. 4113895, pp. 1-13,* view article online.

Tong, Q., Yan, S., Wang, S. and Xue, J., 2022. *"Optimization of Process Technology and Quality Analysis of a New Yogurt Fortified With Morchella Esculenta," Food Science and Technology, Vol. 42, No. e45822,* view article online.

Uchegbulam, I., Salih, A.A. and Obinichi, N. 2019. *"Heat Treatment of UNS T72305 Tool Steel: Effect on Mechanical and Microstructural Properties" The International Journal of Engineering and Science, Vol. 8, No. 9, pp. 50-56.* view article online.